

Structural and Nucleosynthetic Evolution of Metal-poor & Metal-free Low and Intermediate Mass Stars

Simon W. Campbell* and John C. Lattanzio†

*Academia Sinica Institute of Astronomy and Astrophysics, P.O. Box 23-141, Taipei 10617, Taiwan

†Centre for Stellar and Planetary Astrophysics, School of Mathematical Sciences, Monash University, Melbourne, Australia 3800

Abstract. We report on an investigation into stellar evolution and nucleosynthesis in the low and extremely low metallicity regime, including models of stars with a pure Big Bang composition (i.e. $Z = 0$). The metallicity range of the extremely metal-poor (EMP) models we have calculated is $-6.5 < [\text{Fe}/\text{H}] < -3.0$, whilst our models are in the mass range $0.85 < M < 3.0M_{\odot}$. Many of the EMP and $Z = 0$ models experience violent evolutionary episodes not seen at higher metallicities. We refer to these events as ‘Dual Flashes’ since they are characterised by peaks in the hydrogen and helium burning luminosities occurring at roughly the same time. Some of the material processed by these events is later dredged up by the convective envelope, causing significant surface pollution. These events have been reported by previous studies, so our results reaffirm their occurrence – at least in 1D stellar models. The novelty of this study is that we have calculated the entire evolution of the $Z = 0$ and EMP models, from the ZAMS to the end of the TPAGB, including detailed nucleosynthesis. We have also calculated the nucleosynthetic yields, which will soon be available in electronic format. Although subject to many uncertainties these are, as far as we are aware, the only yields available in this mass and metallicity range. In this paper we briefly describe some of the results in the context of abundance observations of EMP halo stars. This work formed part of SWC’s PhD thesis (completed in March 2007) and a series of subsequent papers will describe the results of the study in more detail.

Keywords: Population III, Stellar evolution, Nucleosynthesis, Metal poor halo stars

PACS: 97.10.Cv, 97.20.Wt

MOTIVATION

The discovery of extremely metal-poor stars (EMPs) in the Galactic Halo has renewed interest in the theoretical modelling of Population III and low-metallicity stars. Most of these stars show abundances that conform to a simple Galactic chemical evolution line (see Figure 1). However a subset of the EMP stars have been observed to contain large amounts of carbon. These C-rich EMPs (CEMPs) make up a large proportion of the EMP population ($\sim 10 \rightarrow 20\%$; see eg. [1]). This population is also highlighted in Figure 1. Apart from carbon the EMP stars also display variation in a range of other elements (see [1] for a review of the observations). A number of theories have been proposed to explain the various patterns, ranging from pre-formation pollution via Pop III supernovae (eg. [2], [3]) to self-pollution through peculiar evolutionary events (eg. [4], [5]) to binary mass transfer (eg. [6]).

In the current study we have undertaken a broad exploration of EMP stellar evolution and nucleosynthesis in the low and intermediate mass regime. Our study expands on the previous work in the field. In particular it includes (for the first time) full evolutionary and nucleosynthesis calculations from ZAMS to the end of the thermally-pulsing AGB phase (TPAGB), as well as chemical yields for 74 nuclear species. With this homo-

geneous set of models we hope to shed some light on whether or not 1D stellar models can explain some of the EMP halo star observations.

METHOD

Our simulations were performed utilising two numerical codes – a stellar structure code and post-process nucleosynthesis code.

The stellar structure code used was the Monash/Mount Stromlo STAR code (MONSTAR see eg. [14], [15]). We do not describe the code in detail here but briefly note a few key points. The code is largely a standard 1D code that utilises the Henyey-matrix method (a modified Newton-Raphson method) for solving the stellar structure equations. Opacities have been updated to those from [16] (for mid-range temperatures) and [17] (for low temperatures). For the present study the instantaneous convective mixing routine was replaced by a time-dependent (diffusive) mixing routine (similar to that described by [18]). This change was necessary due to the violent evolutionary events that occur in models of EMP stars. Convective boundaries were always defined by the Schwarzschild criterion – ie. no overshoot was applied. Thus the extension of convective zones in all the models are conservative. A key problem with modelling EMP

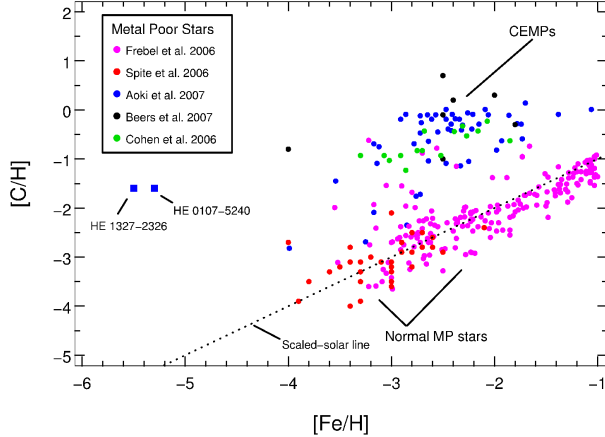


FIGURE 1. Carbon abundance observations versus $[\text{Fe}/\text{H}]$ for metal-poor stars compiled from the literature. The dotted line marks $[\text{C}/\text{Fe}] = 0.0$. The normal EMPs lie on this Galactic chemical evolution line, whilst the CEMPs (which we define as having $[\text{C}/\text{Fe}] > +0.7$) lie above this. The two most Fe-poor stars known, HE 0107-5240 ($[\text{Fe}/\text{H}] = -5.3$, [7]) and HE 1327-2326 ($[\text{Fe}/\text{H}] = -5.4$, [8]) are labelled. We note that this sample is biased towards CEMPs. Observational data sets are from [9], [10], [11], [12], and [13].

stars is the unknown driver(s) of mass loss. The dominant theory is that mass is lost from red giant envelopes through radiation pressure acting on grains. Thus, in the EMP or $Z = 0$ regime, mass loss is thought to be negligible. The MONSTAR code uses empirical mass loss formulae (the formula from [19] during the RGB and that of [20] during the AGB). For this study we chose to retain the standard treatment, for the following reasons. The first is that not much mass is lost during the RGB in these EMP models. This is because their RGB phases are much shorter (or non-existent), since He is ignited much earlier than in stars of comparable mass at higher metallicities. Indeed, the luminosity at the tip of the RGB can be up to 1 order of magnitude lower in EMP models (see eg. [21]). Thus the RGB mass loss is largely negligible, and it is the AGB mass loss that needs to be handled properly. As described in the next Section these models all experience some sort of polluting episode – and always before the AGB phase. This has the consequence that the surface of the AGB models usually have metallicities approaching that of the LMC or even Solar (as defined by Z rather than Fe – they are still metal poor in terms of Fe). Thus, since the stellar surfaces have (some of) the ingredients needed to form grains, we argue that using the standard mass loss formula given by [20] is warranted. We also note that metallicity is also indirectly taken into account by the mass loss formulae, since they depend on bulk stellar properties (such as radius, luminosity, pulsation period), which vary significantly with metallicity.

The nucleosynthesis calculations were made with the Monash Stellar Nucleosynthesis code (MONSN). MONSN is a post-process code. As input it takes the key structural properties of each hydrostatic model from the MONSTAR code (eg. density, temperature, convective velocities). It solves a network of 506 nuclear reactions involving 74 nuclear species (see eg. [22], [23], [24] for more details on this code). Our grid of models covered the mass range: $M = 0.85, 1.0, 2.0, 3.0M_{\odot}$ and the metallicity range: $[\text{Fe}/\text{H}] = -6.5, -5.45, -4.0, -3.0$, plus $Z = 0$.

THE DUAL FLASH EVENTS

It has long been known that theoretical models of $Z = 0$ stars (and EMP stars) undergo violent evolutionary episodes not seen at higher metallicities. This was first suggested by [21] and confirmed by later calculations (see eg. [25], [26], [27]). These episodes occur at different evolutionary stages in stars of different mass and metallicity (see eg. [4]). The most severe of these evolutionary events occurs during the core He flash of low-mass stars (with $[\text{Fe}/\text{H}] < -2.5$, see [4]). In this event the normal flash-driven convective zone breaks out of the He-rich core. Thus H-rich material is mixed down into regions of high temperature. Processed material is also mixed upwards. The proton-rich material burns at a very high rate, amounting to a secondary flash – a H-flash. This flash reaches luminosities comparable to the core He flash itself and occurs within the same time-frame as the He flash. Thus we refer to the combination of these events as a ‘Dual Core Flash’ (DCF). We note that this event has also been referred to as Helium Flash Induced Mixing (HEFM, [28]) and Helium Flash-Driven Deep Mixing (He-FDDM, [6]). A similar event occurs in stellar models of higher mass and higher (although still very low) metallicities. In these cases it is the normal AGB shell He flash-driven convection zone that breaches the H-He discontinuity. This occurs during the first few pulses of the TPAGB phase. Again a H-flash is induced during the evolution of the He-flash, so we refer to this event as a ‘Dual Shell Flash’ (DSF). Both the DCF and DSF events have consequences for the surface composition of the star since, in both cases, the convective envelope subsequently deepens and mixes up the (processed) material overlying the H-burning shell. Presently there is reasonable consensus that these events do indeed occur (at least in stellar models!), although we note that not every study has found them to (eg. [29]). In Figure 2 we display an example calculation of a DCF from one of our models.

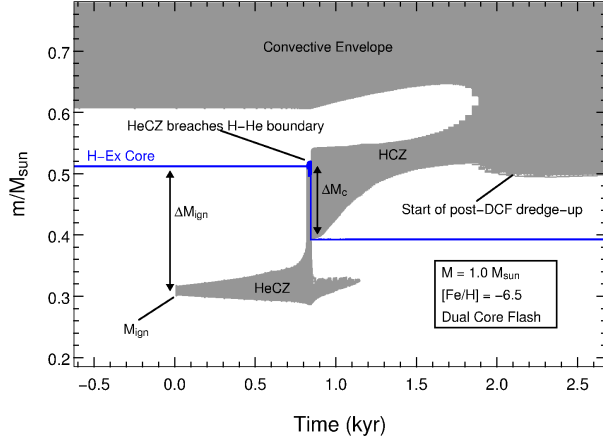


FIGURE 2. An example of one of the Dual Core Flashes that occurred in some of our low metallicity models. In this case it is the $1 M_{\odot}$ model with $[\text{Fe}/\text{H}] = -6.5$. Convective regions are shown by grey shading whilst the mass location of the edge of the H-exhausted core is shown by the solid line (blue). The large inward movement of the H-He boundary (H-Ex. core), due to the ingestion of protons into the HeCZ, can be seen (ΔM_c). The beginning of the post-DCF dredge-up is indicated. This dredge up (mainly of CNO isotopes) increases the surface metallicity to super-solar values (although $[\text{Fe}/\text{H}]$ remains unchanged).

CATEGORISATION OF YIELDS

In Figure 3 we show the results from a nucleosynthesis calculation for one of our models. In this model it is the Third Dredge-Up (3DU – the periodic dredging up of He burning products into the convective envelope) and Hot Bottom Burning (HBB – hydrogen burning at the bottom of the convective AGB envelope) that define the yield of the star. Indeed, the chemical signature arising from the DSF occurring at the start of the AGB is totally erased by these normal AGB evolutionary episodes. However this is not always the case. In Figure 4 we summarise the pollution episodes over the whole grid of models. We group the yields into four categories, defined by the evolutionary events/phases that dominate the chemical signature in the yields: Group 1 yields are dominated by the DCF events, Group 2 are dominated by DSF events, Group 3 are dominated by 3DU+HBB, whilst Group 4 show no surface pollution during their hydrostatic evolution (but may explode as Type 1.5 supernovae). Two key features visible in this figure are (1) members of the DCF group have polluted surfaces during the horizontal branch phase (HB, the core He burning phase) and (2) both the DCF and DSF groups, which are of low mass, have polluted surfaces during the AGB – despite the lack of 3DU. Thus our models predict a greater proportion of C-rich stars at extremely low metallicity, as these events do not occur at higher metallicities.

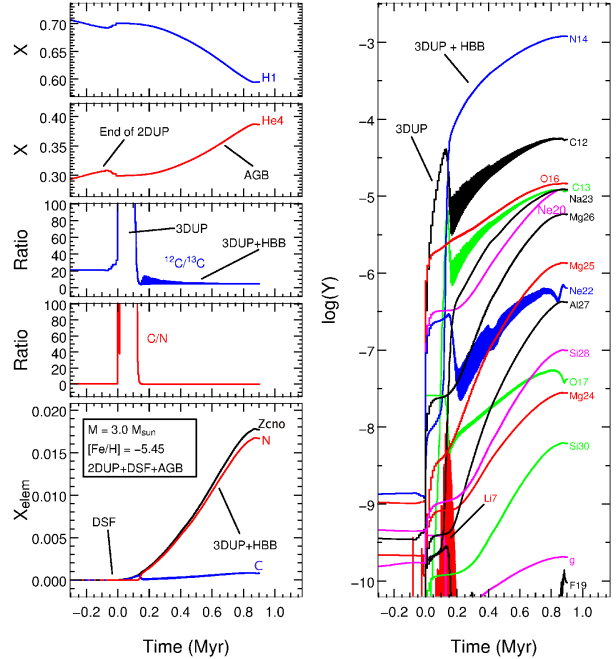


FIGURE 3. The time evolution of the surface composition in the $[\text{Fe}/\text{H}] = -5.45$, $3 M_{\odot}$ model, for selected species. This model fits into our Group 3. The rich nucleosynthesis arising from 3DU and HBB is seen in the right-hand panel. In particular the CN cycling product ^{14}N dominates during most of the AGB. The $^{12}\text{C}/^{13}\text{C}$ and C/N ratios quickly approach equilibrium values once the (strong) HBB starts. This chemical signature by far dominates that of the DSF in this case.

COMPARISONS WITH OBSERVATIONS

In Figure 5 we compare the carbon yields from our entire grid of models with the observed $[\text{C}/\text{Fe}]$ abundances in EMP halo stars. It can be seen that the yields from our models are all C-rich. Moreover, the yields at $[\text{Fe}/\text{H}] = -3$, for which there are the most observations, agree well with the observations. At $[\text{Fe}/\text{H}] = -4$ there is a fair agreement with the observations, although there are less observations to compare with. At $[\text{Fe}/\text{H}] = -5.45$ the yields show somewhat more C than is observed, although there are only two stars observed at this metallicity. An interesting feature of this diagram is that the the model yields predict $[\text{C}/\text{Fe}]$ to continue increasing towards lower metallicities. Furthermore, taking into account the evolutionary stage at which the surface pollution is gained in the lower mass models ($M = 0.85$ and $1.0 M_{\odot}$) – ie. the Dual Core Flash events rather than the AGB – the models also predict a higher proportion of C-rich stars at lower and lower metallicities. This is due to the fact that these stars already have polluted surfaces during the HB stage – which has a lifetime roughly 1 order of magnitude longer than the AGB phase. The

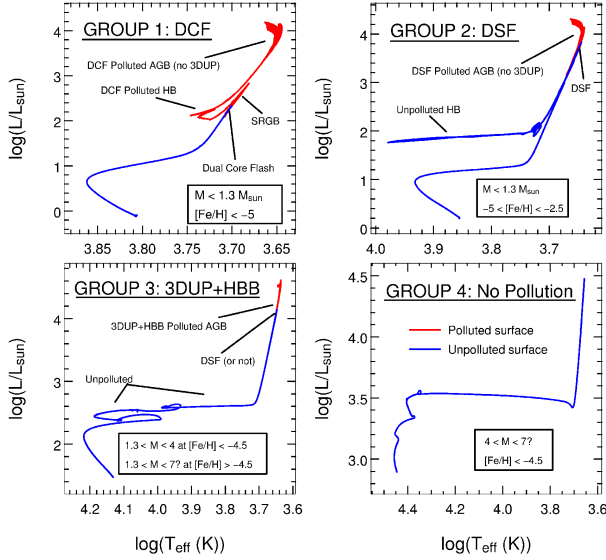


FIGURE 4. Displayed in each HR diagram is a representative example from our grid of models for each pollution group. Grey (red) lines indicate phases of the evolution in which the surface is strongly polluted with CNO nuclides (from the DCF, DSF or 3DU events). Black (blue) lines indicate that the surface still retains the initial metal-poor composition. Evolutionary stages and pollution sources are marked, as are the mass and metallicity ranges of each group. Question marks indicate unknown upper boundaries (due to the limited mass range of the current study).

CEMPs also show interesting behaviour in other elemental abundances. In Figure 6 we compare the integrated yields from our $[\text{Fe}/\text{H}] = -5.45$ models with the observed abundance patterns of the two most metal-poor halo stars. Apart from N these two stars show similar abundance patterns. They both have roughly the same C and O abundances and, although offset to lower abundances, the Na and Mg abundances follow the same pattern. Nitrogen is 2 dex more abundant in HE 1327-2326. The dominance of N over (enhanced) C and O in HE 1327-2326 is reminiscent of the pattern that CNO cycling plus 3DU creates. This pattern is also seen in the yields of the $2 M_{\odot}$ and $3 M_{\odot}$ models. In these models it is 3DU+HBB that dominates the chemical signature of the yields. It may be possible that HE 1327-2326 has been polluted by an intermediate mass AGB star that had undergone 3DU and partial (or lower temperature) HBB. Na and Mg are very much overproduced in these models compared to the observations but, again, lower temperature or incomplete HBB may account for this. HE 0107-5240 on the other hand is better ‘matched’ (it is still far from ideal) by the $1 M_{\odot}$ yield. The yield of this model is dominated by the DSF event at the start of the AGB. In this case N and Na are overproduced in the model relative to the observations.

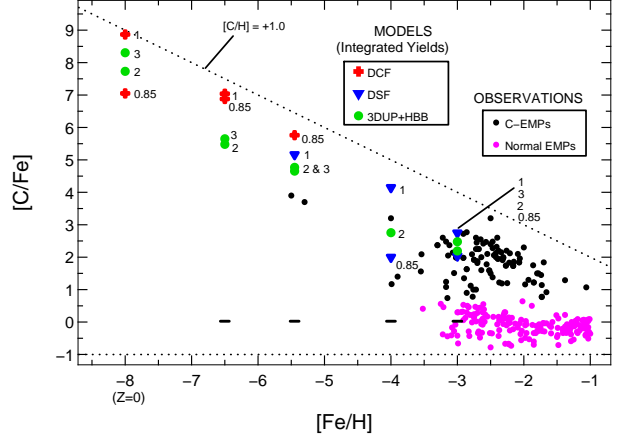


FIGURE 5. Comparing the yields from all our models with observations of EMP stars. See Figure 1 for the observational data sources. Here we have colour-coded the observations into $[\text{C}/\text{Fe}]$ -rich (black dots) and $[\text{C}/\text{Fe}]$ -normal (grey/magenta dots), where $[\text{C}/\text{Fe}]$ -rich is defined by $[\text{C}/\text{Fe}] > +0.7$. The short horizontal lines indicate the starting composition of the models (in this case they are all at $[\text{C}/\text{Fe}] \sim 0$, except for the $Z = 0$ models). We have plotted the $Z = 0$ model yields at $[\text{Fe}/\text{H}] = -8$ for comparison. The two most metal-poor stars can be seen at $[\text{Fe}/\text{H}] \sim -5.5$ (they are both C-rich). An upper envelope to the pollution of the models – and the observations – is marked by the dotted line at $[\text{C}/\text{H}] = +1.0$. The yields from our models are colour- and shape-coded to highlight the different episodes that produced the bulk of the pollution in each yield. Numbers beside each yield marker indicate initial stellar mass, in M_{\odot} .

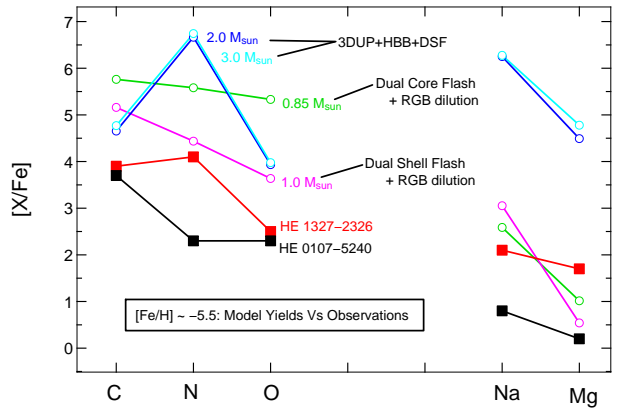


FIGURE 6. Comparing the abundance pattern in our $[\text{Fe}/\text{H}] = -5.45$ yields (open circles, initial stellar masses as indicated) with observations of stars with the same metallicity (closed squares). The abundance determinations in these stars are from [8] (HE 1327-2326) and [7] (HE 0107-5240).

More comparisons and analysis will be reported in future papers arising from this thesis.

SUMMARY

In agreement with most previous studies we find that many of the EMP and $Z = 0$ models experience violent evolutionary episodes not seen at higher metallicities. We refer to these events as ‘Dual Flashes’ (DFs).

The models predict an increased number of carbon-rich stars at the lowest metallicities. This is mainly due to the extra pollution provided by the DF events. This concurs well with the observations, which show the proportion of CEMP stars in the Galactic halo to be higher at lower metallicities. Although not discussed here we also note that we found the pollution arising from the DF events to be simultaneously C- and N-rich, as also observed in the CEMP stars. This contrasts with the pollution expected from 3DU at low mass, which would be (mainly) C-rich. Furthermore, the models predict that the proportion of CEMP stars should *continue* to increase at lower metallicities, based on the results that the low mass EMP models already have polluted surfaces by the HB phase, and that there are more C-producing evolutionary episodes at these metallicities. We also compared the chemical pollution arising from the models with the detailed abundance patterns available for some of the most metal-poor CEMP stars, and found mixed results.

We note that all these calculations contain many uncertainties. These include the unknown mass-loss rates, uncertain nuclear reaction rates, and the treatment of convection. In the case of the DF events a further uncertainty is the possibility that full fluid dynamics calculations are really needed to model these violent episodes.

The models and yields from this thesis will be described in more detail in a series of future papers. For interested readers a full version of the thesis is available on SWC’s webpage.

ACKNOWLEDGMENTS

Most of the calculations for this study utilised the Australian Partnership for Advanced Computing’s supercomputer, under Project Code *g6I*. SWC thanks the original authors and maintainers of the stellar codes that have been used in this thesis – Peter Wood, Rob Cannon, John Lattanzio, Maria Lugaro, Amanda Karakas, Cheryl Frost, Don Faulkner and Bob Gingold. SWC was supported by a Monash University Research Graduate School PhD scholarship for 3.5 years.

REFERENCES

1. T. Beers, and N. Christlieb, *ARA&A* **43**, 531–580 (2005).
2. T. Shigezumi, and T. Tsujimoto, *ApJL* **507**, L135–L139 (1998).

3. M. Limongi, A. Chieffi, and P. Bonifacio, *ApJL* **594**, L123–L126 (2003).
4. M. Y. Fujimoto, Y. Ikeda, and I. J. Iben, *ApJ* **529**, L25–L28 (2000).
5. A. Weiss, H. Schlattl, M. Salaris, and S. Cassisi, *A&A* **422**, 217–223 (2004).
6. T. Suda, M. Aikawa, M. N. Machida, M. Y. Fujimoto, and I. J. Iben, *ApJ* **611**, 476–493 (2004).
7. N. Christlieb, B. Gustafsson, A. J. Korn, P. S. Barklem, T. C. Beers, M. S. Bessell, T. Karlsson, and M. Mizuno-Wiedner, *ApJ* **603**, 708–728 (2004).
8. W. Aoki, A. Frebel, N. Christlieb, J. E. Norris, T. C. Beers, T. Minezaki, P. S. Barklem, S. Honda, M. Takada-Hidai, M. Asplund, S. G. Ryan, S. Tsangarides, K. Eriksson, A. Steinhauer, C. P. Deliyannis, K. Nomoto, M. Y. Fujimoto, H. Ando, Y. Yoshii, and T. Kajino, *ApJ* **639**, 897–917 (2006).
9. A. Frebel, N. Christlieb, J. E. Norris, T. C. Beers, M. S. Bessell, J. Rhee, C. Fechner, B. Marsteller, S. Rossi, C. Thom, L. Wisotzki, and D. Reimers, *ApJ* **652**, 1585–1603 (2006).
10. M. Spite, R. Cayrel, V. Hill, F. Spite, P. François, B. Plez, P. Bonifacio, P. Molaro, E. Depagne, J. Andersen, B. Barbuy, T. C. Beers, B. Nordström, and F. Primas, *A&A* **455**, 291–301 (2006).
11. W. Aoki, T. C. Beers, N. Christlieb, J. E. Norris, S. G. Ryan, and S. Tsangarides, *ApJ* **655**, 492–521 (2007).
12. T. C. Beers, T. Sivarani, B. Marsteller, Y. Lee, S. Rossi, and B. Plez, *AJ* **133**, 1193–1203 (2007).
13. J. G. Cohen, A. McWilliam, S. Shectman, I. Thompson, N. Christlieb, J. Melendez, S. Ramirez, A. Swenson, and F.-J. Zickgraf, *AJ* **132**, 137–160 (2006).
14. P. R. Wood, and D. M. Zarro, *ApJ* **247**, 247–256 (1981).
15. C. A. Frost, and J. C. Lattanzio, *ApJ* **473**, 383 (1996).
16. C. A. Iglesias, and F. J. Rogers, *ApJ* **464**, 943 (1996).
17. J. W. Ferguson, D. R. Alexander, F. Allard, T. Barman, J. G. Bodnarik, P. H. Hauschildt, A. Heffner-Wong, and A. Tamanai, *ApJ* **623**, 585–596 (2005).
18. G. Meynet, A. Maeder, and N. Mowlavi, *A&A* **416**, 1023–1036 (2004).
19. D. Reimers, *Memoires of the Societe Royale des Sciences de Liege* **8**, 369–382 (1975).
20. E. Vassiliadis, and P. R. Wood, *ApJ* **413**, 641–657 (1993).
21. F. Dantona, *A&A* **115**, L1–L3 (1982).
22. R. C. Cannon, *MNRAS* **263**, 817 (1993).
23. J. Lattanzio, C. Frost, R. Cannon, and P. R. Wood, *MmSAI* **67**, 729 (1996).
24. M. Lugaro, C. Ugalde, A. I. Karakas, J. Görres, M. Wiescher, J. C. Lattanzio, and R. C. Cannon, *ApJ* **615**, 934–946 (2004).
25. M. Y. Fujimoto, I. J. Iben, and D. Hollowell, *ApJ* **349**, 580–592 (1990).
26. D. Hollowell, I. J. Iben, and M. Y. Fujimoto, *ApJ* **351**, 245–257 (1990).
27. S. Cassisi, V. Castellani, and A. Tornambe, *ApJ* **459**, 298 (1996).
28. H. Schlattl, M. Salaris, S. Cassisi, and A. Weiss, *A&A* **395**, 77–83 (2002).
29. L. Siess, M. Livio, and J. Lattanzio, *ApJ* **570**, 329–343 (2002).